

Supplementary Data

VDAC1 is a Molecular Target in Glioblastoma, with Its Depletion Leading to Reprogrammed Metabolism and Reversed Oncogenic Properties

Tasleem Arif*, Yakov Kerlin*, Itay Nakdimon, Daniel Benharroch, Avijit Paul, Daniela Dadon-Klein and Varda Shoshan-Barmatz

Materials and Methods

Materials

The cell transfection agents JetPRIME and JetPEI were obtained from PolyPlus transfection (Illkirch, France), while non-modified and 2'-O-methyl-modified hVDAC1-siRNAs were obtained from Genepharma (Suzhou, China). Bovine serum albumin (BSA), carbonyl cyanide-p-trifluoromethoxyphenylhydrazone (FCCP), Polyethylenimine (PEI), Poly(D,L-lactide-co-glycolide) (PLGA), Polyvinyl alcohol (PVA), propidium iodide (PI), sulforhodamine B (SRB), Triton X-100, Tween-20, tetramethylrhodamine methylester (TMRM), hematoxylin, eosin, and itraconazole were obtained from Sigma (St. Louis, MO). Paraformaldehyde was purchased from Emsdiasum (Hatfield, PA). Dulbecco's modified Eagle's medium (DMEM), and Roswell Park Memorial Institute (RPMI) 1640 growth media, BSA (7.5%), non-essential amino acids (NEAA) and B27 and N2 supplements were obtained from Gibco (Grand Island, NY). DMEM/HAMS-F12, Minimum essential media (MEM), normal goat serum (NGS), fetal calf serum (FCS) and the supplements L-glutamine and penicillin-streptomycin were obtained from Biological Industries (Beit Haemek, Israel). Human EGF and FGF were purchased from Millipore (Billerica, MA). A cancer stem cell TF activation profiling plate array was obtained from Signosis (Santa Clara, CA). Primary antibodies, their source and the dilutions used are detailed in Supplementary Table S1. Horseradish peroxidase (HRP)-conjugated anti-mouse, anti-rabbit and anti-goat antibodies were from KPL (Gaithersburg, MD). A CellTiter-Glo luciferase-based assay and TUNEL stain was obtained from Promega (Madison, WI). Nuclear/cytosol fractionation kit was obtained from (Biovision, Milpitas, CA). 3,3-diaminobenzidine (DAB) was obtained from (ImmPact-DAB, Burlingame, CA).

Cell culture and transfection

U-87MG, U-251MG, U-118MG, LN-18 (human glioblastoma), human glioblastoma patient-derived cells MZ-18 and MZ-327¹, kindly provided by D. Kogel, University Hospital, Frankfurt, Germany, C6 (rat glioma), GL-261 (mouse glioma), and non-cancerous HaCat (spontaneously transformed aneuploid immortal keratinocyte cell line from adult human skin), were maintained in DMEM culture medium supplemented with 10% FBS (5% for LN18), 1 mM L-glutamine, 100 U/ml penicillin, and 100 µg/ml streptomycin. U-251MG (human glioblastoma) cells cultured in RPMI-1640 medium supplemented with 10% FBS, 1 mM L-glutamine, 100U/ml penicillin, and 100 µg/ml streptomycin at 37°C and 5% CO₂. Cells of the glioma-derived G7 stem cell line were grown using specific glioblastoma stem cell medium, as described previously². HUVEC (human umbilical vein cells) were cultured in complete EGM-2 medium (Lonza, Walkersville, MD, USA). Primary astrocyte and glia cells were prepared as described previously³. Newborn 2-3 days old mice (C57Bl/6) were sacrificed using CO₂ and their brains were quickly removed and digested with 0.25% trypsin for 15

min at 37°C. The cell suspension was centrifuged through a 10% FCS solution and the obtained cells were grown in DMEM with 10% FCS, 5% CO₂ at 37°C.

The following siRNA sequences were used, with 2'-O-methyl-modified nucleotides indicated in bold and underlined (nucleotide positions are provided for sense (S) and anti-sense (AS) sequences): si-hVDAC12/A, S: 238-5'- ACACUAGGCACCCGAGAUU A-3'-256 and AS: 5'- UAAUCUCGGUGCCUAGGUGU -3' and si-NT, S: -5'-GCAAACAUCCCAGAGGUAU-3' and AS: 5'-AUA CCUCUGGGAUGUUUGC-3'; hVDAC1A, S: 159-5'-GGGCUAUGGAUUUGGCUU A-3'-177 and AS: 5'-UAAGCCAAAUCCAUAAG CCC-3'; VDAC1B, S: 337-5'ACACUAGGCACCG AGAUUA-3'-355 and AS: 5'-UAAUCUCGGUGCCUA GUGU-3'; VDAC1C, S: 921-5'-GCUUGGUCU AGGACUGGAA-3'-939 and AS: 5'-UCCAGUCCUAGACCAAGC-3'; VDAC1M/H, S: 487-5'-GAAUAGCAGCCAAGUAUCA GTT-3'-505 and AS: 5'-UGA UACUUGGCUGCUAUUCTT-3'. Cells were seeded (100,000- 150,000 cells/well) in 6-well culture dishes to 40-60% confluence and transfected with 10-60 nM si-NT or si-hVDAC1 using the JetPRIME transfection reagent (Illkirch, France), according to the manufacturer's instructions. U-87MG cells were transiently transfected with plasmid pcDNA4/TO (2 µg DNA) encoding native mVDAC1 using the JetPRIME reagent according to the manufacturer's instructions.

Sulforhodamine B (SRB) assay for cell proliferation

Twenty-four hours post-transfection with non-targeting siRNA (si-NT) or modified si-hVDAC1, U-87MG, U-118MG, U-251MG, LN-18, cells were counted and seeded in 96-well plates. For rat C6 glioma and mouse GL261 glioma, mouse- and human-specific siRNA (VDAC1M/H) were used. The cells were counted and seeded in 96-well plates.

To assess the effect of itraconazole on cell growth, HUVEC, U-87MG, U-118MG, LN-18 and mouse primary brain cells (PBCs) were seeded in 96-well plates (2,000 cells/ well), allowed to attach overnight and then incubated with itraconazole (0.1 to 10 µM) for 24 hours. The final DMSO concentration in control and itraconazole-containing samples was 0.5%. Cells were washed with PBS, fixed with 10% trichloroacetic acid for 1-2 h, and subsequently stained with sulforhodamine B (SRB). SRB was extracted from the cells using 100 mM Tris base and absorbance at 510 nm was determined using an Infinite M1000 plate reader (Tecan, Männedorf, Switzerland).

Mitochondrial membrane potential determination

Mitochondrial membrane potential ($\Delta\Psi$) was determined using tetramethylrhodamine methylester (TMRM) dye. U-87MG cells were transfected with si-NT or si-hVDAC1 and 48 h post-transfection, were incubated with TMRM (700 nM, 30 min) and washed with PBS. TMRM fluorescence was measured with an Infinite M1000 plate reader. FCCP served as a control for $\Delta\Psi$ dissipation.

Determination of cellular ATP levels

Cellular ATP levels were estimated using a luciferase-based assay (CellTiter-Glo, Promega). U-87MG cells were transfected with si-NT or si-hVDAC1 and 36 h post-transfection were washed twice with PBS and seeded in 96-well plates at densities of 5×10^4 cells/ml. ATP levels were assayed according to the manufacturer's protocol and luminescence was recorded using an Infinite M1000 plate reader (Tecan, Männedorf, Switzerland).

Xenograft and intracranial-orthotopic mouse models

U-87MG glioblastoma cells (2×10^6) were inoculated s.c. into the hind leg flanks of athymic eight-week old male nude mice (Harlan). Eleven days post-inoculation, tumor volume was measured ($50\text{--}80 \text{ mm}^3$) and mice were randomized into two groups (9 animals/group), treated with si-NT or si-hVDAC1 mixed with *in vivo* JetPEI reagent and injected into the established s.c. tumors (50 nM final, 2 boluses) every three days. At the end of the experiments, the mice were sacrificed, tumors were excised, and half of each tumor was either fixed and processed for IHC or frozen in liquid nitrogen for later immunoblot and RNA isolation.

For the intracranial-orthotopic mouse model, U-87MG cells were treated with 50 nM si-NT or si-hVDAC1 twice at a 4-day interval and engrafted into a nude mouse brain using a stereotactic device. The anesthetized mice were immobilized in a stereotactic head frame (Stoelting, Wood Dale, IL) and an incision was made on the skull and a burr hole 0.5 mm anterior to the bregma and 2.0 mm lateral to the midline was made using a drill (Stoelting). A 31-gauge needle loaded with 10 μL phosphate-buffered saline (PBS) was used to deliver tumor cells. The needle tip was inserted into the brain 3-mm deep, relative to the skull surface, and maintained at this depth for 1 minute before injection of tumor cells. Under sterile conditions, a 3 μL solution containing U-87MG (8×10^4) cells was injected into the brain parenchyma over a period of 3 minutes using an UltraMicroPump III (World Precision Instruments, Sarasota, FL). After infusion, the needle was left in place for 1 minute before slow withdrawal. The burr hole was sealed using sterile bone wax, and the wound was closed with 5.0 nylon surgical suture. All surgical procedures were performed under sterile conditions⁴. At the end of the experiment, mice were sacrificed, and their brains were excised and processed for IHC.

The experimental protocols used were approved by the Institutional Animal Care and Use Committee.

MRI tumor monitoring

In vivo brain MRI was performed using the M7 1-Tesla compact ICON system (Aspect Imaging, M7, Israel), equipped with a set of application-specific radiofrequency (RF) 20-mm mouse head coils. For *in vivo* imaging, animals were maintained in an anesthetized state with 1.5% isoflurane in O_2 and placed on a specially designed heated bed where physiological signals, such as breath rate, were monitored throughout the experiment to ensure the animals' well-being. MRI acquisition parameters included fast spin echo with a repetition time of 2,500 ms and echo time of 74 ms. Fifteen axial slices of 0.25 mm with a gap of 0.1 and a matrix of 256X256, field of view of 40 mm and acquisition time of 14.3⁵ were collected. Data were analyzed by VivoQuant 2.10 software.

PLGA encapsulation of siRNA

VDAC1 siRNA-loaded PEI-PLGA complexes were prepared by the solvent displacement method with some modifications, as previously reported⁶. A pre-formed complex of PEI (20 mg) dissolved in 1% of polyvinyl alcohol (PVA) and siRNA 360 μl of siRNA solution (50 μM) was incubated for 30 min at 37°C. PLGA (50 mg) was dissolved in 1 ml acetone. To this organic mixture, 10 ml of aqueous solution containing 1% PVA (w/v) stabilizer was added in a drop-wise manner (0.5 ml/min). Subsequently, the pre-formed complexes containing siRNAs were added in a drop-wise manner. The mixtures were stirred continuously at room temperature until complete evaporation of the organic solvent. The nanoparticles were centrifuged at 15,000g (4°C for 30 min) and the pellet was re-suspended in DEPC-water, washed three times and the resulting nanoparticles containing the siRNA-loaded suspension was stored at -20°C until further use.

TUNEL assay

Fixed tumor sections in paraffin were processed for the TUNEL assay using the DeadEnd Fluorometric TUNEL system (Promega, Madison, WI) according to the manufacturer's instructions. Sections were deparaffinized, equilibrated in PBS, permeabilized with proteinase K (20 µg/ml in PBS), post-fixed in 4% paraformaldehyde, and incubated in TdT reaction mix (Promega) for 1 h at 37°C in the dark. Slides were then washed in 2x saline-sodium citrate (SSC) buffer and counterstained with propidium iodide (1 µg/ml), and cover slipped with Vectashield mounting medium (Vector Laboratories, Burlingame, CA). Fluorescent images of apoptotic cells (green) and cell nuclei (red) were captured using a confocal microscope (Olympus 1X81).

Immunoblot

For immunostaining, membranes containing electro-transferred proteins following SDS-PAGE were blocked with 5% non-fat dry milk and 0.1% Tween-20 in TBS, incubated with the primary antibodies (sources and dilutions as detailed in Supplementary Table S1) and then with HRP-conjugated anti-mouse or anti-rabbit (1:10,000) or anti-goat (1:20,000) IgG. Enhanced chemiluminiscent substrate (Pierce Chemical, Rockford, IL) was used for detection of HRP activity.

Immunohistochemistry (IHC) and immunofluorescence of tumor tissue sections

Immunohistochemical and immunofluorescence staining was performed on 5 µm-thick formalin-fixed and paraffin-embedded tumor tissue sections. The sections were deparaffinized by placing the slides at 60°C for 1 h and using xylene. Thereafter, the tissue sections were rehydrated with a graded ethanol series (100%-50%). Antigen retrieval for some proteins (VDAC1, Glut1, citrate synthases, HK-II, GAPDH, LDH, Nestin, NGFR, KLF4, Sox2, S100b, Musashi, Map2, b-III tubulin (TUBB3), GAD67, ATP5a, cytochrome c oxidase subunit VIc, c-Kit, N-cadherin, E-cadherin, vimentin) was performed in 0.01 M citrate buffer (pH 6.0). For HK-I and CD31, VEGF, Ki-67, GFAP, F4/80, HNF4, FOXP1, NRSF/Rest, MAZ, antigen retrieval was performed in 10 mM Tris-EDTA (pH 9) and 0.5 M Tris (pH 10) for 30 minutes each at 95-98°C. After washing sections in PBS containing 0.1% Triton-X100 (pH 7.4), non-specific antibody binding was reduced by incubating the sections in 10% NGS for 2 h. After decanting excess serum, sections were incubated overnight at 4°C with primary antibodies (sources and dilutions used detailed in Supplementary Table S1). Sections were washed with PBST. For IHC, endogenous peroxidase activity was blocked by incubating the sections in 3% H₂O₂ for 15 min. After washing thoroughly with PBST, the sections were incubated for 2 h with anti-mouse or anti rabbit (1:250) secondary antibodies conjugated to HRP were used, as appropriate. Sections were washed five times in PBST and the peroxidase reaction was subsequently visualized by incubating with 3,3-diaminobenzidine (DAB) (ImmPact-DAB, Burlingame, CA). After rinsing in water, the sections were counterstained with hematoxylin, and mounted with mounting medium. Finally, the sections were observed under a microscope (Leica DM2500) and images were collected at 20× magnification with the same light intensity and exposure time. Non-specific control experiments were carried out using the same protocols but omitting incubation with the primary antibodies. For immunofluorescence, Cy3-conjugated anti-rabbit (1:500) or Cy2-conjugated anti-mouse (1:200) secondary antibodies were used. The cells were then stained with DAPI (0.07 µg/ml) and viewed with an Olympus IX81 confocal microscope.

RNA preparation and DNA microarray analysis

Total RNA was isolated from si-NT- and si-hVDAC1-treated tumors (4-6 mice each) using an RNeasy mini kit (Qiagen) according to the manufacturer's instructions. Total RNA quality was analyzed using the Agilent RNA 6000 nano kit. The RNA integrity values obtained for total RNA extracted from si-NT- and si-hVDAC1-treated tumors were 8-10, respectively. The targets for Affymetrix whole transcript expression microarray analyses were prepared using the Affymetrix GeneChip WT PLUS reagent kit according to the manufacturer's instructions and hybridized to Human Gene 1.0 ST microarrays. Data were acquired using the Affymetrix GeneChip algorithm (version 3.2). CEL files were imported to Partek Genomics Suite and all probes except control probes were pre-processed by RMA background correction, log₂ transformation and probe set summarization using median polish. Probe sets with signals < 5 in all samples were filtered out. Subsequently, global scaling was carried out by shifting the mean of each sample to the grand mean (i.e. in each sample, the mean signal was subtracted from each of the signals, and then the grand mean from all samples was added, such that all arrays eventually had the same mean signal). Differentially expressed genes were defined as those having FDR-adjusted a t test p-value < 0.05, and two clusters were defined, up-regulated and down-regulated genes (linear fold change > 2 and < -2, respectively). Each cluster was tested separately for enrichment of functional groups based on the GO system. Promoter analysis was performed using the DAVID and Expander⁷ software tools.

Quantitative real-time PCR

Real-time RT-PCR was performed using specific primers (KiCqStart Primers; Sigma Aldrich) in triplicate, using Power SYBER green master mix (Applied Biosystems, Foster City, CA). Levels of target genes were normalized relative to β -actin mRNA levels. Samples were amplified by a 7300 Real Time PCR System (Applied Biosystems) for denaturation step of 5 min at 95°C and 40 cycles using the following PCR parameters: 95°C for 15 seconds, 60°C for 1 minute, and 72°C for 1 minute. The copy numbers for each sample were calculated by the CT-based calibrated standard curve method. The mean fold changes (\pm SEM) of the three replicates were calculated. Genes examined and primers used are listed in Supplementary Table S2.

TF profiling array

Nuclear extracts were prepared from si-NT- or si-hVDAC1-treated tumors using a Nuclear/cytosol fractionation kit (Biovision, Milpitas, CA) following the manufacturer's instructions. TF DNA-binding activity was analyzed as per the manufacturer's instructions (Signosis, Sunnyvale, CA). Briefly, a nuclear extract (~13 μ g of protein) was added to a mixture of DNA sequences encoding 23 different TF-binding sites (BS) and incubated at 16°C for 30 min. The samples containing the formed TF-DNA complexes were then separated from free DNA probes using an isolation column, with an aliquot (100 μ l) being applied to the column and TF-DNA complexes being eluted with elution buffer (200 μ l). A sample (95 μ l) was then added to each well of a 96-well plate containing an immobilized complementary sequence to one of the 23 TFs. The plate was sealed and incubated overnight at 42°C for hybridization. The plate was then washed three times, and developed using streptavidin conjugated-HRP and luminescence obtained following substrate addition was recorded using an Infinite M1000 microplate reader.

Neurosphere formation

Conditions for neurosphere formation were as described previously⁸. Briefly, U-87MG, G7, MZ-18 and MZ-327 cells were treated with si-NT or si-hVDAC1 (50 nM) and 24 h post-transfection, the cells (10⁵) were cultured in 12-well plates coated with a soft agar (5%) layer prepared in neuronal stem cell medium, as described previously². Following 24 h incubation at 37°C in a 5% CO₂ atmosphere, the cultures were photographed.

VDAC1 purification and channel conductance measurement

VDAC1 protein was purified from rat liver mitochondria as previously described⁹. The reconstitution of purified rat VDAC1 into a planar lipid bilayer (PLB) and subsequent single and multiple channel current recordings and data analysis were also carried out as previously described^{10,11}. Briefly, a PLB was prepared from soybean asolectin dissolved in n-decane (30 mg/ml). Purified VDAC1 (1 ng) was added to the chamber defined as the *cis* side containing 1 M NaCl, 10 mM Hepes, pH 7.4. Currents were recorded under voltage-clamp using a Bilayer Clamp BC-535B amplifier (Warner Instruments, Hamden, CT). The currents, measured with respect to the *trans* side of the membrane (ground), were low-pass-filtered at 1 kHz and digitized online using a Digidata1440-interface board and pClampex 10.2 software (Axon Instruments, Union City, CA).

Itraconazole interaction with VDAC1 using the microscale thermophoresis (MST) analysis

MST analysis was performed using a NanoTemper Monolith NT.115 apparatus as described previously¹². Briefly, purified VDAC1 was fluorescently labeled using a NanoTemper Protein labeling kit BLUE (L001, NanoTemper Technologies). A constant concentration of the protein was incubated with different concentrations of the tested inhibitor in PBS. Afterwards, 3-5 µl of the samples were loaded into a glass capillary (Monolith NT Capillaries) and thermophoresis analysis was performed (LED 20%, IR laser 20%).

Supplementary Tables

Table S1. Antibodies used in this study

Antibodies against the indicated protein, their catalogue number, source, and the dilutions used in IHC, immunoblot and immunofluorescence experiments are presented.

Antibody	Source and Cat. No.	Dilution		
		IHC	WB	IF
Mouse monoclonal anti-actin	Millipore, Billerica, MA, MAB1501	-	1:10000	-
Mouse monoclonal anti-ATP5a	Abcam, Cambridge, UK, ab14748	1:300	1:1000	-
Mouse monoclonal anti-β III tubulin	Abcam, Cambridge, UK ab7751	1:100	1:1000	1:200
Rabbit polyclonal anti-CD31	Abcam, Cambridge, UK ab28364	1:50		-
Rabbit polyclonal anti-CD44	Abcam, Cambridge, UK ab157107	1:1000	1:3000	-
Mouse monoclonal anti-CD133	Miltenyi Biotec GmbH , AC133	-	1:1500	-
Rabbit polyclonal anti-citrate synthase	Abcam, Cambridge, UK ab96600	1:200	1:4000	-
Rabbit polyclonal anti c-Kit	Dako, CL, USA, A4502	1:400	-	-
Mouse monoclonal anti-cytochrome c	BD Bioscience, San Jose, CA, 556432	1:400	1:2000	-

Rabbit monoclonal cytochrome c oxidase subunit VIc	Abcam, Cambridge, UK, ab150422	1:200	1:2000	-
Rabbit polyclonal anti EGFR	Abcam, Cambridge, UK, ab2430	1:300	1:2000	-
Mouse monoclonal anti-E-cadherin	Invitrogen ,Life Technologies, NY,18-0223	1:100	1:1000	-
Rat monoclonal anti-F4/80	Santa Cruz Biotechnology, Inc. Dallas, TX, sc52664	1:150	-	-
Rabbit polyclonal anti-FoxP1	Abcam, Cambridge, UK, ab191184	1:300	1:1500	-
Mouse monoclonal anti-GAPDH	Abcam, Cambridge, UK, ab9484	1: 200	1:1000	-
Mouse monoclonal anti-GAD67	Abcam, Cambridge, UK, ab26116	-	1:2000	1:1500
Mouse monoclonal anti-GFAP	Santa Cruz Biotechnology, Inc. Dallas, TX, sc-33673	1:200	1:1000	1:150
Rabbit monoclonal anti-Glut1	Abcam, Cambridge, UK ab40084	1: 200	1: 1500	-
Mouse monoclonal anti-HK-I	Abcam, Cambridge, UK ab105213	1:500	1:2000	-
Rabbit polyclonal anti-HKII	Abcam, Cambridge, UK ab3279	1:400	1:2000	-
Rabbit polyclonal ant-HNF4	Abcam, Cambridge, UK, ab92378	1:300	1:1000	-
Rabbit monoclonal anti-Ki67	Thermo Scientific, NY RM-9106-s1	1:100	-	-
Rabbit polyclonal anti-KLF4	IMGEX Littleton, USA, IMG-6081-A	1:200	1:1000	-
Rabbit monoclonal anti-LDH	Epitomics, Cambridge, UK, 1980-1	1:300	1:1000	-
Goat polyclonal anti-LDH-A	Santa Cruz Biotechnology, Inc. Dallas, TX, sc-27230	-	1:1500	-
Mouse monoclonal anti-Map2	Sigma-Aldrich, St. Louis, MI, M 4403	1:400	-	-
Rabbit polyclonal anti-Maz	Abcam, Cambridge, UK , ab114965	1:300	-	-
Mouse monoclonal anti-Musashi-1	Millipore, Billerica, MA, MABE268	1:200	-	-
Mouse monoclonal anti-N-cadherin	Invitrogen (Life Technologies), NY 18-0224	1:200	-	-
Rabbit polyclonal anti-Nestin	Millipore, Billerica, MA, MAB353	1:400	1:1000	1:1500
Rabbit polyclonal anti -NGFR	Santa Cruz Biotechnology, Inc. Dallas, TX, sc-8317	1:200	1:1000	-
Rabbit polyclonal anti NRSF/Rest	Abcam, Cambridge, UK , ab70300	1:200	-	-
Mouse monoclonal anti-P53	Santa Cruz Biotechnology, Inc. ,Dallas, TX, sc-126	-	1:5000	-
Goat polyclonal anti-S100b	Millipore, Billerica, MA, ABN59	1:300	1:2000	-
Goat polyclonal anti-Sox2	Santa Cruz Biotechnology, Inc. Dallas, TX, sc-17320	1:200	1:1500	-
Rabbit monoclonal anti-VDAC1	Abcam, Cambridge, UK , ab154856	1:500	1:5000	-
Mouse monoclonal anti -VEGF	Santa Cruz Biotechnology, Inc. Dallas, TX. sc-65617	1:50	1:1000	-
Mouse monoclonal anti-Vimentin	Invitrogen, Life Technologies, NY 18-0052	1:300	1:1000	-

Table S2: Real-Time PCR primers used in this study

The genes examined, and the forward and reverse sequences of the primers used are indicated.

Gene	Primer sequences
<i>β-Actin</i>	Forward 5'-ACTCTTCCAGCCTTCCTTCC-3' Reverse 5'-TGTTGGCGTACAGGTCTTTG-3'
<i>ALDH1L1</i>	Forward 5'-CCAAAGTCCTGGAGGTTGAA-3' Reverse 5'-TAACTCCAGGCCATCACACA-3'
<i>BLPB (FABP7)</i>	Forward 5'-AGTTTCCAGCTGGGAGAAGAG-3' Reverse 5'-CTTTGCCATCCCATTCTGTGA-3'
<i>CS</i>	Forward 5'-AGGAACAGGTATCTTGGCTCT-3' Reverse 5'-GGGGTGTAGATTGGTGGGAA-3'
<i>c-Myc</i>	Forward 5'-GTAGTGGAAAACCAGCAGCC-3' Reverse 5'-CCTCCTCGTCGCAGTAGAAA-3'
<i>GFAP</i>	Forward 5'-AAGCTCCAGGATGAAACCAAC-3' Reverse 5'-AGCGACTCAATCTTCCTCTCC-3'
<i>GAPDH</i>	Forward 5'-TGGAAGGACTCATGACCACA-3' Reverse 5'-ATGATGTTCTGGAGAGCCCC-3'
<i>GLUT1</i>	Forward 5'-GGCCATCTTTTCTGTTGGGG-3' Reverse 5'-TCAGCATTGAATTCCGCCG-3'
<i>Hif-1α</i>	Forward 5'-CTGACCCTGCACTCAATCAA-3' Reverse 5'-TCCATCGGAAGGACTAGGTG-3'
<i>HK-1</i>	Forward 5'-GTCTCAGTCCAGCACGTTTG-3' Reverse 5'-GAAACGCCGGAATACTGTG-3'
<i>Ki-67</i>	Forward 5'-CTTTGGGTGCGACTTGACG-3' Reverse 5'-GTCGACCCCGCTCCTTTT-3'
<i>LDH-A</i>	Forward 5'-GCAGGTGGTTGAGAGTGCTT-3' Reverse 5'-GCACCCGCCTAAGATTCTTC-3'
<i>MAP2</i>	Forward 5'-TCCAAAATCGGATCAACAGAC-3' Reverse 5'-AGAGCCACATTTGGATGTCAC-3'
<i>Nanog</i>	Forward 5'-TGGGATTTACAGGCGTGAGCCAC-3' Reverse 5'-AAGCAAAGCCTCCCAATCCCAAAC-3'
<i>N-cadherin</i>	Forward 5'-AGGGATCAAAGCCTGGAACA-3' Reverse 5'-TTGGAGCCTGAGACACGATT-3'
<i>Nestin</i>	Forward 5'-GAAACAGCCATAGAGGGCAAA-3' Reverse 5'-TGTTTTCCAGAGTCTTCAGTGA-3'
<i>Oct-3/4</i>	Forward 5'-GGGCTCTCCCATGCATTCAAAC-3' Reverse 5'-CACCTTCCCTCCAACAGTTGC-3'
<i>PCNA</i>	Forward 5'-GCCGAGATCTCAGCCATATT-3' Reverse 5'-ATGTACTIONAGAGGTACAAAT-3'
<i>Snail1</i>	Forward 5'-AGTGGTTCTTCTGCGCTACT-3' Reverse 5'-CTGCTGGAAGGTAAACTCTGG-3'
<i>Snail2 (SLUG)</i>	Forward 5'-ACATACAGTGATTATTTCCCCGT-3' Reverse 5'-CGCCCCAAAGATGAGGAGTA-3'
<i>SOX10</i>	Forward 5'-AGGAGAGGTCCGAGGAGGTG-3' Reverse 5'-CTCAGCTCCACCTCCGATAG-3'
<i>p53</i>	Forward 5'-AGGTTGGCTCTGACTGTACC-3' Reverse 5'-AAAGCTGTTCCGTCACAGTA-3'
<i>SOX2</i>	Forward 5'-CCATGCAGGTTGACACCGTTG-3' Reverse 5'-TCGGCAGACTGATTCAAATAA-3'

<i>SSEA-1(CD15)</i>	Forward 5'-TGAAATAGCTTAGCGGCAAGA-3' Reverse 5'-GTGAATCGGGAACAGTTGTGT-3'
<i>Tnc</i>	Forward 5'-ATGAATCAGTGGATGGCACA-3' Reverse 5'-CCATTGAGTGCCTGGATCTT-3'
<i>TUBB3</i>	Forward 5'-CTCAGGGGCCTTTGGACATC-3' Reverse 5'-CAGGCAGTCGCAGTTTTTCAC-3'
<i>Twist</i>	Forward 5'-TCTTACGAGGAGCTGCAGAC-3' Reverse 5'-TATC CAGCTCCAGAGTCTCT-3'
<i>Zeb1</i>	Forward 5'- TTCCTGAGGCACCTGAAGAG-3' Reverse 5'- GGTGTTCCATTTTCATCATGACC-3'
<i>Zeb2</i>	Forward 5'-TAGTGTGCCCAACCATGAGT-3' Reverse 5'- TTGCATTCTTCACTGGACCA-3'

Table S3. List of selected genes differentially expressed between si-NT- and si-hVDAC1-treated tumors, as identified by DNA microarray analysis

Selected genes from the down-regulated (cluster 1) and up-regulated (cluster 2) groups (see Fig. 6), representing major functional groups, i.e. associated with cell cycle, DNA repair, metabolism (TCA cycle, oxidative phosphorylation), regulation of gene expression, Wnt signaling or neuronal differentiation, are presented. For each gene, the gene symbol and name, fold change in expression and p-value are indicated. Negative numbers reflect down-regulation.

	si-hVDAC1- vs. si-NT-treated tumors		
Gene	Fold-Change	p-value	Function
Cluster 1, down-regulated genes			
<i>Cellular metabolism and survival regulation</i>			
EGFR-Epidermal growth factor receptor	-2.78	4.9E-03	EGF receptor, activates the oncogenic Ras signaling cascade ¹³
MDM2-p53 binding protein homolog	-7.97	2.2E-03	ligase, regulates p53 level via degradation ¹⁴
HIF1 α -Hypoxia inducible factor 1, alpha subunit	-13.34	2.2E-03	Transcription factor, master regulator of response to hypoxia ¹⁵
<i>Cell cycle</i>			
CCNB1-cyclin B1	-4.61	1.9E-03	Essential for the control of the cell cycle at G2/M (mitosis) ¹⁶
CCNG1-cyclin G1	-19.46	2.8E-05	Associated with G2/M phase arrest in response to DNA damage in the TP53 pathway ¹⁷
<i>DNA repair</i>			
ATM-serine/threonine kinase	-3.10	3.8E-03	Activates checkpoint signaling upon double strand breaks ¹⁸
BRCA2-Breast cancer 2	-4.20	8.9E-04	Involved in double-strand break repair and/or homologous recombination ¹⁹
TP53BP1-Tumor protein p53 binding protein 1	-3.10	1.3E-03	Enhances TP53-mediated transcriptional activation ²⁰
TP53BP2-Tumor p53 binding protein 2	-2.35	1.6E-03	Regulates TP53 by enhancing its DNA binding ²⁰
<i>TCA cycle</i>			
IDH3A-Isocitrate dehydrogenase 3 alpha subunit	-9.00	6.1E-04	TCA cycle enzyme involved in energy production ²¹
SDHB-Succinate dehydrogenase	-4.86	4.5E-03	Involved in energy production ²²

complex, subunit B,			
<i>Oxidative phosphorylation</i>			
NDUFB6-NADH dehydrogenase (ubiquinone) 1 beta sub-complex, 6,	-4.69	3.0E-04	Electron transport component, energy production ²³
ATP5B-ATP synthase, beta subunit	-2.77	1.0E-03	Uses mitochondrial $\Delta\Psi$ for ATP synthesis ²⁴
COX6C-Cytochrome c oxidase, subunit VIc	-11.29	2.5E-03	Electron transport component, energy production ²⁵
Cluster 2, up-regulated genes			
<i>Negative regulation of gene expression</i>			
ID4-Inhibitor of DNA binding 4	6.10	4.4E-03	Does not bind DNA directly, rather inhibits activity of other transcription factors ²⁶
FOXP4-Forkhead box P4	5.20	9.2E-03	Transcriptional repressor that represses lung-specific expression ²⁷
<i>Wnt signaling</i>			
FZD1-Frizzled homolog 1	4.47	8.2E-03	Receptor for Wnt proteins ²⁸
WNT1-Wingless-type MMTV integration site family, member 1	6.19	4.8E-03	Ligand for members of the frizzled family receptors ²⁹
<i>Neuron differentiation</i>			
UNC5B-homolog B, Netrin receptor	2.88	1.4E-03	A netrin-1 receptor, thought to mediate the netrin-1 chemorepulsive effect ³⁰
CDK5R1-cyclin-dependent kinase 5, regulatory subunit 1 (p35)	6.11	3.5E-04	Involved in proper development of the central nervous system ³¹
MANF-Mesencephalic astrocyte-derived neurotrophic factor	4.48	9.2E-04	Involved in ER stress-induced death and cell proliferation ³²

Table S4. List of selected genes associated with tumor oncogenic properties differentially expressed in si-NT- and si-hVDAC1-treated tumors, as identified by DNA microarray analysis

Selected genes whose expression changed and are associated with invasion, including metalloproteinases (MMP) and inhibitors of their transcription, extra-cellular matrix proteins (EMC) and integrin and angiogenesis, are listed, as is their function. For each gene, fold change in expression, p-value and function are indicated. Negative numbers reflect down-regulation.

Invasive related genes	si-hVDAC1- vs. si-NT-treated tumors		Function
	Fold Change	p-value	
<i>MMP transcription and function inhibitors</i>			
ID4-inhibitor of DNA binding 4	6.10	4.4E-04	Transcriptional negative regulator of basic helix-loop-helix TFs ²⁶
TIMP1-metalloproteinase inhibitor 1	-5.80	9.0E-05	Inhibitor of several MMPs, including MMP-3, MMP7-13 and MMP16 ³³
TIMP2-metalloproteinase inhibitor 2	-4.00	3.4E-03	Inhibitor of several MMPs, including MMP-1-3, 7-10, 13-16, 19 ³⁴
TIMP3-metalloproteinase inhibitor 3	-4.71	2.3E-03	Inhibitor of several MMPs, including MMP-1-3, 7,9,13-15 ³⁵
<i>MMP proteins</i>			
MMP2-matrix metalloproteinase 2	-7.9	2.3E-03	Metalloproteinase cleaving gelatin type I and collagen types IV, V, VII, X ³⁶

MMP16- matrix metalloproteinase 16	-2.3	7.9E-03	Metalloproteinase cleaving collagen type III and fibronectin ³⁷
ADAM9-Disintegrin and metalloproteinase domain-containing protein 9	-11.0	5.0E-04	Membrane-anchored zinc protease implicated in cell-cell and cell-matrix interactions ³⁸
ADAM12-Disintegrin and metalloproteinase domain-containing protein 12	-7.1	6.0E-04	Membrane-anchored zinc protease involved in cell-cell and cell-matrix interactions ³⁹
<i>ECM and integrin genes</i>			
LAMB1-laminin, beta 1 chain	-4.2	9.0E-03	Component of the ECM ⁴⁰
LAMC1-laminin, gamma 1	-5.1	6.6E-04	Component of the ECM ⁴¹
ITGA2-integrin, alpha 2	-4.9	2.6E-04	Mediates cell matrix and cell-cell interactions ⁴²
ITGA3-integrin, alpha 3 (subunit of VLA-3)	-7.4	5.3E-04	Mediates cell matrix and cell-cell interactions ⁴³
ITGA5-integrin, alpha 5 (fibronectin receptor)	-4.2	4.7E-03	Mediates cell matrix and cell-cell interactions ⁴⁴
ITGB1BP1-integrin beta 1 binding protein 1	-4.2	3.7E-04	Mediates cell matrix and cell-cell interactions ⁴⁵
ITGB3BP-integrin beta 3 binding protein	-6.6	1.2E-03	Mediates cell matrix and cell-cell interactions ⁴⁶
CD44-Hyaluronic acid receptor	-3.1	3.8E-04	Receptor for hyaluronic acid ⁴⁷
CD99-Transmembrane glycoprotein	-9.0	2.1E-04	Inhibits cell-extracellular matrix adhesion ⁴⁸
CD164-Sialomucin core protein 24 (endolyn)	-21.2	2.1E-04	Cell adhesion molecule ⁴⁹
<i>Angiogenesis</i>			
VEGFB-Vascular endothelial growth factor B	4.5	3.4E-04	Growth factor for endothelial cells of newly formed blood vessels ⁵⁰
VEGFC-Vascular endothelial growth factor C	-2.1	6.3E-05	Growth factor for lymphatic endothelial cells ⁵¹
NRP1-Neuropilin 1	-4.7	1.8E-04	Membrane co-receptor for both VEGF and Semaphorin, also functions in axon guidance, cell survival, migration, and invasion ⁵²
TGFB1-Transforming growth factor, beta 1	-3.1	2.3E-04	Growth factor controlling proliferation, differentiation and more cell functions ⁵³
TGFBR1-Transforming growth factor, beta receptor 1	-2.2	1.1E-03	Co-receptor for TGFBR2 activated by bound TGFβ ⁵⁴
TGFBR2-Transforming growth factor, beta receptor 2	-6.7	1.5E-04	Constitutively active co-receptor TGFBR1 of bound TGFβ ⁵⁵
CD109- tumor endothelial cells marker	-12.3	2.0E-04	GPI-linked cell surface antigen ⁵⁶
<i>Angiogenic inhibitors</i>			
HIF1AN-hypoxia inducible factor 1, alpha subunit inhibitor	-2.3	6.8E-04	Preventing interaction of HIF-1 with transcriptional co-activators ⁵⁷
SERPINF1-Serpin peptidase inhibitor, clade F	2.3	9.2E-03	Inhibitor of neovascularization and tumorigenesis and activator of neurotrophic functions ⁵⁸
THBS1-Thrombospondin 1	10.4	3.2E-03	Inhibitor of neovascularization and tumorigenesis ⁵⁹

Table S5. Master TFs, p53, HIF1-a and c-Myc, and their regulation of tumor oncogenic properties via a panel of other TFs

The indicated TFs levels were analyzed in si-NT- and si-hVDAC1-TTs using q-RT-PCR, immunoblotting, IHC staining or DNA microarray analysis.

Master TF	Regulated TF	Oncogenic properties	Reference
p53	Klf4, Oct3/4, c-Myc	Stemness	60
	Sox2, Nanog, Oct3/4	Stemness	61
	Snail1	EMT	62
	Twist*	EMT	63
	Zeb 1, 2	EMT	64
HIF1-α	Sox2, Oct3/4, Nanog, Klf4	Stemness	65
	Snail, Twist	EMT	66
	Zeb1	EMT	67
	NRSF	Neuronal differentiation suppressor	68
	Foxp1	Oncogene/Tumor suppressor	69
c-Myc	Sox2	Stemness	70
	Nanog**, Klf4**, Oct3/4	Stemness	71-73
	Snail	EMT	74
	Twist	EMT	75
	NRSF	Neuronal differentiation suppressor	76
	FOXP1	Oncogene/Tumor suppressor	77
	MAZ	Differentiation suppressor	78

*Twist is involved in the regulation of p53 activation

**Nanog and Klf4 are involved in the regulation of c-Myc transcription function

Supplemental References

1. Hetschko H, Voss V, Horn S, Seifert V, Prehn JH, Kogel D. Pharmacological inhibition of Bcl-2 family members reactivates TRAIL-induced apoptosis in malignant glioma. *Journal of neuro-oncology*. Feb 2008;86(3):265-272.
2. Pollard SM, Yoshikawa K, Clarke ID, et al. Glioma stem cell lines expanded in adherent culture have tumor-specific phenotypes and are suitable for chemical and genetic screens. *Cell Stem Cell*. Jun 5 2009;4(6):568-580.
3. Shabtay-Orbach A, Amit M, Binenbaum Y, Na'ara S, Gil Z. Paracrine regulation of glioma cells invasion by astrocytes is mediated by glial-derived neurotrophic factor. *Int J Cancer*. Sep 1 2015;137(5):1012-1020.
4. Pierce AM, Keating AK. Creating anatomically accurate and reproducible intracranial xenografts of human brain tumors. *Journal of visualized experiments : JoVE*. 2014(91):52017.
5. Tempel-Brami C, Schiffenbauer YS, Nyska A, et al. Practical Applications of in Vivo and ex Vivo MRI in Toxicologic Pathology Using a Novel High-performance Compact MRI System. *Toxicol Pathol*. Jul 2015;43(5):633-650.
6. Das J, Das S, Paul A, Samadder A, Bhattacharyya SS, Khuda-Bukhsh AR. Assessment of drug delivery and anticancer potentials of nanoparticles-loaded siRNA targeting STAT3 in lung cancer, in vitro and in vivo. *Toxicol Lett*. Mar 21 2014;225(3):454-466.
7. Ulitsky I, Maron-Katz A, Shavit S, et al. Expander: from expression microarrays to networks and functions. *Nature protocols*. 2010;5:303-322.
8. Rota LM, Lazzarino DA, Ziegler AN, LeRoith D, Wood TL. Determining mammosphere-forming potential: application of the limiting dilution analysis. *J Mammary Gland Biol Neoplasia*. Jun 2012;17(2):119-123.
9. Ben-Hail D, Shoshan-Barmatz V. Purification of VDAC1 from rat liver mitochondria. *Cold Spring Harb Protoc*. Jan 2014;2014(1):94-99.
10. Ben-Hail D, and Shoshan-Barmatz, V. Reconstitution of purified VDAC1 into a lipid bilayer and recording of channel conductance. *Cold Spring Harb Protoc*. 2014b:100-105.
11. Ben-Hail D, Shoshan-Barmatz V. Reconstitution of purified VDAC1 into a lipid bilayer and recording of channel conductance. *Cold Spring Harb Protoc*. Jan 2014b;2014(1):100-105.
12. Wienken CJ, Baaske P, Rothbauer U, Braun D, Duhr S. Protein-binding assays in biological liquids using microscale thermophoresis. *Nat Commun*. 2010;1:100.
13. Shih C, Shilo BZ, Goldfarb MP, Dannenberg A, Weinberg RA. Passage of phenotypes of chemically transformed cells via transfection of DNA and chromatin. *Proc Natl Acad Sci U S A*. Nov 1979;76(11):5714-5718.
14. Momand J, Zambetti GP. Mdm-2: "big brother" of p53. *J Cell Biochem*. Mar 1 1997;64(3):343-352.
15. Wang GL, Jiang BH, Rue EA, Semenza GL. Hypoxia-Inducible Factor-1 Is a Basic-Helix-Loop-Helix-Pas Heterodimer Regulated by Cellular O-2 Tension. *P Natl Acad Sci USA*. Jun 6 1995;92(12):5510-5514.
16. Pines J, Hunter T. Cyclins A and B1 in the human cell cycle. *Ciba Found Symp*. 1992;170:187-196; discussion 196-204.
17. Okamoto K, Kamibayashi C, Serrano M, Prives C, Mumby MC, Beach D. p53-dependent association between cyclin G and the B' subunit of protein phosphatase 2A. *Mol Cell Biol*. Nov 1996;16(11):6593-6602.
18. Rotman G, Shiloh Y. The ATM gene and protein: possible roles in genome surveillance, checkpoint controls and cellular defence against oxidative stress. *Cancer Surv*. 1997;29:285-304.
19. Zhang H, Tomblin G, Weber BL. BRCA1, BRCA2, and DNA damage response: collusion or collusion? *Cell*. Feb 20 1998;92(4):433-436.
20. Iwabuchi K, Li B, Massa HF, Trask BJ, Date T, Fields S. Stimulation of p53-mediated transcriptional activation by the p53-binding proteins, 53BP1 and 53BP2. *J Biol Chem*. Oct 2 1998;273(40):26061-26068.
21. Bzymek KP, Colman RF. Role of alpha-Asp181, beta-Asp192, and gamma-Asp190 in the distinctive subunits of human NAD-specific isocitrate dehydrogenase. *Biochemistry*. May 8 2007;46(18):5391-5397.

22. Bardella C, Pollard PJ, Tomlinson I. SDH mutations in cancer. *Biochim Biophys Acta*. Nov 2011;1807(11):1432-1443.
23. Ling C, Poulsen P, Simonsson S, et al. Genetic and epigenetic factors are associated with expression of respiratory chain component NDUFB6 in human skeletal muscle. *J Clin Invest*. Nov 2007;117(11):3427-3435.
24. Ahmad Z, Okafor F, Azim S, Laughlin TF. ATP synthase: a molecular therapeutic drug target for antimicrobial and antitumor peptides. *Curr Med Chem*. 2013;20(15):1956-1973.
25. Hofmann S, Lichtner P, Schuffenhauer S, Gerbitz KD, Meitinger T. Assignment of the human genes coding for cytochrome c oxidase subunits Va (COX5A), VIc (COX6C) and VIIc (COX7C) to chromosome bands 15q25, 8q22-->q23 and 5q14 and of three pseudogenes (COX5AP1, COX6CP1, COX7CP1) to 14q22, 16p12 and 13q14-->q21 by FISH and radiation hybrid mapping. *Cytogenet Cell Genet*. 1998;83(3-4):226-227.
26. Rahme GJ, Israel MA. Id4 suppresses MMP2-mediated invasion of glioblastoma-derived cells by direct inactivation of Twist1 function. *Oncogene*. Jan 2 2015;34(1):53-62.
27. Teufel A, Wong EA, Mukhopadhyay M, Malik N, Westphal H. FoxP4, a novel forkhead transcription factor. *Biochim Biophys Acta*. Jun 19 2003;1627(2-3):147-152.
28. Flahaut M, Meier R, Coulon A, et al. The Wnt receptor FZD1 mediates chemoresistance in neuroblastoma through activation of the Wnt/beta-catenin pathway. *Oncogene*. Jun 11 2009;28(23):2245-2256.
29. Cadigan KM, Peifer M. Wnt signaling from development to disease: insights from model systems. *Cold Spring Harb Perspect Biol*. Aug 2009;1(2):a002881.
30. Thiebault K, Mazelin L, Pays L, et al. The netrin-1 receptors UNC5H are putative tumor suppressors controlling cell death commitment. *Proc Natl Acad Sci U S A*. Apr 1 2003;100(7):4173-4178.
31. Mateo I, Vazquez-Higuera JL, Sanchez-Juan P, et al. Epistasis between tau phosphorylation regulating genes (CDK5R1 and GSK-3 beta) and Alzheimer's disease risk. *Acta Neurol Scand*. Aug 2009;120(2):130-133.
32. Lindholm P, Saarma M. Novel CDNF/MANF family of neurotrophic factors. *Dev Neurobiol*. Apr 2010;70(5):360-371.
33. Sreekanthreddy P, Srinivasan H, Kumar DM, et al. Identification of potential serum biomarkers of glioblastoma: serum osteopontin levels correlate with poor prognosis. *Cancer epidemiology, biomarkers & prevention : a publication of the American Association for Cancer Research, cosponsored by the American Society of Preventive Oncology*. Jun 2010;19(6):1409-1422.
34. Fillmore HL, VanMeter TE, Broaddus WC. Membrane-type matrix metalloproteinases (MT-MMPs): expression and function during glioma invasion. *Journal of neuro-oncology*. Jun 2001;53(2):187-202.
35. Jackson HW, Hojilla CV, Weiss A, Sanchez OH, Wood GA, Khokha R. Timp3 deficient mice show resistance to developing breast cancer. *PloS one*. 2015;10(3):e0120107.
36. Gong J, Zhu S, Zhang Y, Wang J. Interplay of VEGFa and MMP2 regulates invasion of glioblastoma. *Tumour biology : the journal of the International Society for Oncodevelopmental Biology and Medicine*. Dec 2014;35(12):11879-11885.
37. Li Y, Wang Y, Yu L, et al. miR-146b-5p inhibits glioma migration and invasion by targeting MMP16. *Cancer letters*. Oct 10 2013;339(2):260-269.
38. Formolo CA, Williams R, Gordish-Dressman H, MacDonald TJ, Lee NH, Hathout Y. Secretome signature of invasive glioblastoma multiforme. *Journal of proteome research*. Jul 1 2011;10(7):3149-3159.
39. Kodama T, Ikeda E, Okada A, et al. ADAM12 is selectively overexpressed in human glioblastomas and is associated with glioblastoma cell proliferation and shedding of heparin-binding epidermal growth factor. *The American journal of pathology*. Nov 2004;165(5):1743-1753.
40. Khazenzon NM, Ljubimov AV, Lakhter AJ, et al. Antisense inhibition of laminin-8 expression reduces invasion of human gliomas in vitro. *Molecular cancer therapeutics*. Oct 2003;2(10):985-994.
41. Fowler A, Thomson D, Giles K, et al. miR-124a is frequently down-regulated in glioblastoma and is involved in migration and invasion. *European journal of cancer*. Apr 2011;47(6):953-963.

42. Bernhart E, Damm S, Wintersperger A, et al. Protein kinase D2 regulates migration and invasion of U87MG glioblastoma cells in vitro. *Experimental cell research*. Aug 1 2013;319(13):2037-2048.
43. Li XL, Lu X, Parvathaneni S, et al. Identification of RECQ1-regulated transcriptome uncovers a role of RECQ1 in regulation of cancer cell migration and invasion. *Cell cycle*. 2014;13(15):2431-2445.
44. Mallawaarachy DM, Buckland ME, McDonald KL, et al. Membrane proteome analysis of glioblastoma cell invasion. *Journal of neuropathology and experimental neurology*. May 2015;74(5):425-441.
45. Cheng TY, Wu MS, Lin JT, et al. Annexin A1 is associated with gastric cancer survival and promotes gastric cancer cell invasiveness through the formyl peptide receptor/extracellular signal-regulated kinase/integrin beta-1-binding protein 1 pathway. *Cancer*. Dec 1 2012;118(23):5757-5767.
46. van Roosmalen W, Le Devedec SE, Golani O, et al. Tumor cell migration screen identifies SRPK1 as breast cancer metastasis determinant. *J Clin Invest*. Apr 1 2015;125(4):1648-1664.
47. Pietras A, Katz AM, Ekstrom EJ, et al. Osteopontin-CD44 signaling in the glioma perivascular niche enhances cancer stem cell phenotypes and promotes aggressive tumor growth. *Cell Stem Cell*. Mar 6 2014;14(3):357-369.
48. Shintaku M, Yoneda H, Hirato J, Nagaishi M, Okabe H. Gliosarcoma with ependymal and PNET-like differentiation. *Clinical neuropathology*. Nov-Dec 2013;32(6):508-514.
49. Shi JA, Lu DL, Huang X, Tan W. miR-219 inhibits the proliferation, migration and invasion of medulloblastoma cells by targeting CD164. *International journal of molecular medicine*. Jul 2014;34(1):237-243.
50. Zhang F, Tang Z, Hou X, et al. VEGF-B is dispensable for blood vessel growth but critical for their survival, and VEGF-B targeting inhibits pathological angiogenesis. *Proc Natl Acad Sci U S A*. Apr 14 2009;106(15):6152-6157.
51. Carpenter RL, Paw I, Zhu H, et al. The gain-of-function GLI1 transcription factor TGLI1 enhances expression of VEGF-C and TEM7 to promote glioblastoma angiogenesis. *Oncotarget*. Jun 4 2015.
52. Hamerlik P, Lathia JD, Rasmussen R, et al. Autocrine VEGF-VEGFR2-Neuropilin-1 signaling promotes glioma stem-like cell viability and tumor growth. *The Journal of experimental medicine*. Mar 12 2012;209(3):507-520.
53. Frei K, Gramatzki D, Tritschler I, et al. Transforming growth factor-beta pathway activity in glioblastoma. *Oncotarget*. Mar 20 2015;6(8):5963-5977.
54. Pineda MJ, Lu Z, Cao D, Kim JJ. Influence of Cancer-Associated Endometrial Stromal Cells on Hormone-Driven Endometrial Tumor Growth. *Hormones & cancer*. Aug 2015;6(4):131-141.
55. Ye XZ, Xu SL, Xin YH, et al. Tumor-associated microglia/macrophages enhance the invasion of glioma stem-like cells via TGF-beta1 signaling pathway. *Journal of immunology*. Jul 1 2012;189(1):444-453.
56. Zhang JM, Murakumo Y, Hagiwara S, et al. CD109 attenuates TGF-beta1 signaling and enhances EGF signaling in SK-MG-1 human glioblastoma cells. *Biochemical and biophysical research communications*. Apr 3 2015;459(2):252-258.
57. Wang E, Zhang C, Polavaram N, et al. The role of factor inhibiting HIF (FIH-1) in inhibiting HIF-1 transcriptional activity in glioblastoma multiforme. *PloS one*. 2014;9(1):e86102.
58. Zhang T, Guan M, Xu C, Chen Y, Lu Y. Pigment epithelium-derived factor inhibits glioma cell growth in vitro and in vivo. *Life sciences*. Sep 29 2007;81(16):1256-1263.
59. Choi SH, Tamura K, Khajuria RK, et al. Antiangiogenic variant of TSP-1 targets tumor cells in glioblastomas. *Molecular therapy : the journal of the American Society of Gene Therapy*. Feb 2015;23(2):235-243.
60. Ren D, Wang M, Guo W, et al. Wild-type p53 suppresses the epithelial-mesenchymal transition and stemness in PC-3 prostate cancer cells by modulating miR145. *International journal of oncology*. Apr 2013;42(4):1473-1481.
61. Betaneli V, Petrov EP, Schwille P. The role of lipids in VDAC oligomerization. *Biophys J*. Feb 8 2012;102(3):523-531.
62. Zheng H, Kang Y. Multilayer control of the EMT master regulators. *Oncogene*. Apr 3 2014;33(14):1755-1763.

63. Ansieau S, Morel AP, Hinkal G, Bastid J, Puisieux A. TWISTing an embryonic transcription factor into an oncoprotein. *Oncogene*. Jun 3 2010;29(22):3173-3184.
64. Kim T, Veronese A, Pichiorri F, et al. p53 regulates epithelial-mesenchymal transition through microRNAs targeting ZEB1 and ZEB2. *The Journal of experimental medicine*. May 9 2011;208(5):875-883.
65. Mathieu J, Zhang Z, Zhou W, et al. HIF induces human embryonic stem cell markers in cancer cells. *Cancer research*. Jul 1 2011;71(13):4640-4652.
66. Hung JJ, Yang MH, Hsu HS, Hsu WH, Liu JS, Wu KJ. Prognostic significance of hypoxia-inducible factor-1alpha, TWIST1 and Snail expression in resectable non-small cell lung cancer. *Thorax*. Dec 2009;64(12):1082-1089.
67. Joseph JV, Conroy S, Pavlov K, et al. Hypoxia enhances migration and invasion in glioblastoma by promoting a mesenchymal shift mediated by the HIF1alpha-ZEB1 axis. *Cancer letters*. Apr 1 2015;359(1):107-116.
68. Formisano L, Guida N, Valsecchi V, et al. Sp3/REST/HDAC1/HDAC2 Complex Represses and Sp1/HIF-1/p300 Complex Activates ncx1 Gene Transcription, in Brain Ischemia and in Ischemic Brain Preconditioning, by Epigenetic Mechanism. *The Journal of neuroscience : the official journal of the Society for Neuroscience*. May 13 2015;35(19):7332-7348.
69. Wan L, Huang J, Chen J, et al. Expression and significance of FOXP1, HIF-1a and VEGF in renal clear cell carcinoma. *Journal of B.U.ON. : official journal of the Balkan Union of Oncology*. Jan-Feb 2015;20(1):188-195.
70. Wong DJ, Liu H, Ridky TW, Cassarino D, Segal E, Chang HY. Module map of stem cell genes guides creation of epithelial cancer stem cells. *Cell Stem Cell*. Apr 10 2008;2(4):333-344.
71. Marzi I, Cipolleschi MG, D'Amico M, et al. The involvement of a Nanog, Klf4 and c-Myc transcriptional circuitry in the intertwining between neoplastic progression and reprogramming. *Cell cycle*. Jan 15 2013;12(2):353-364.
72. Akita H, Marquardt JU, Durkin ME, et al. MYC activates stem-like cell potential in hepatocarcinoma by a p53-dependent mechanism. *Cancer research*. Oct 15 2014;74(20):5903-5913.
73. Kim J, Chu J, Shen X, Wang J, Orkin SH. An extended transcriptional network for pluripotency of embryonic stem cells. *Cell*. Mar 21 2008;132(6):1049-1061.
74. Smith AP, Verrecchia A, Faga G, et al. A positive role for Myc in TGFbeta-induced Snail transcription and epithelial-to-mesenchymal transition. *Oncogene*. Jan 22 2009;28(3):422-430.
75. Selmi A, de Saint-Jean M, Jallas AC, et al. TWIST1 is a direct transcriptional target of MYCN and MYC in neuroblastoma. *Cancer letters*. Feb 1 2015;357(1):412-418.
76. Singh SK, Kagalwala MN, Parker-Thornburg J, Adams H, Majumder S. REST maintains self-renewal and pluripotency of embryonic stem cells. *Nature*. May 8 2008;453(7192):223-227.
77. Craig VJ, Cogliatti SB, Imig J, et al. Myc-mediated repression of microRNA-34a promotes high-grade transformation of B-cell lymphoma by dysregulation of FoxP1. *Blood*. Jun 9 2011;117(23):6227-6236.
78. Bossone SA, Asselin C, Patel AJ, Marcu KB. MAZ, a zinc finger protein, binds to c-MYC and C2 gene sequences regulating transcriptional initiation and termination. *Proc Natl Acad Sci U S A*. Aug 15 1992;89(16):7452-7456.

Supplementary Figures

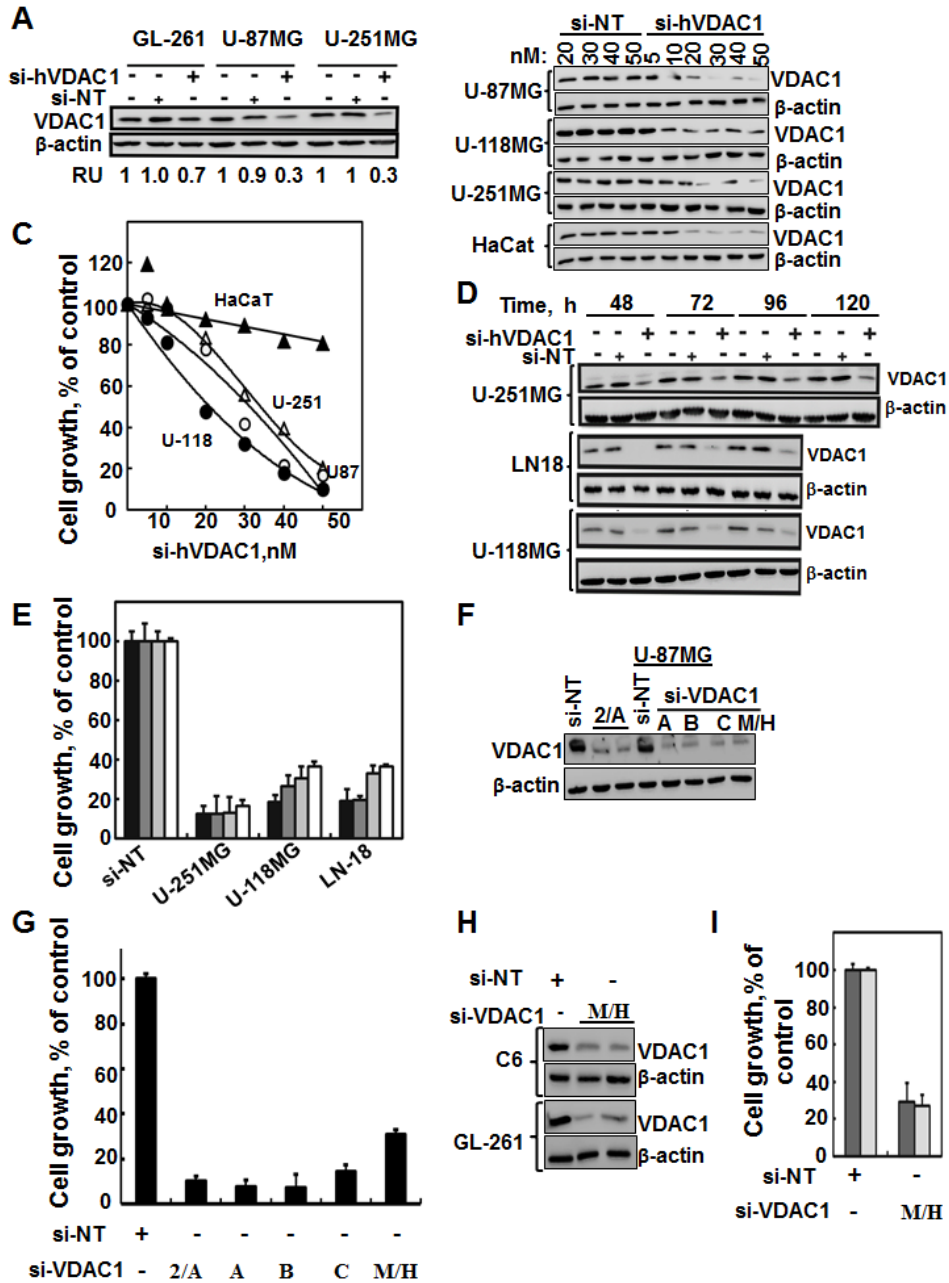


Figure S1. si-VDAC1 silences VDAC1 expression and inhibits cell growth in several human glioblastoma cell lines but to lesser extents in non-cancerous cells

(A) Immunoblot of murine GL-261 and human U-87MG and U-251MG cells treated for 48h with si-NT or si-hVDAC. (B,C) GBM U-118MG and U-251MG cells and non-cancerous, HaCat cells were treated with si-NT or si-hVDAC1 (5-50 nM) and 48 h post-transfection, the cells were analyzed for VDAC1 expression levels (B) and cell growth using the SRB method (C). (D,E) U-251MG, LN-18 and U-118MG (human glioblastoma) cells were treated for the indicated times with si-NT or si-hVDAC1 (50 nM) and at the indicated time were analyzed for VDAC1 levels (D) by immunoblotting or analyzed for cell growth at the indicated time using the SRB (E) method (n=3), 48h (black bars), 72h (gray bars), 96h (light gray bars) and 120h (white bars). (F, G) U-87MG cells were treated with 50 nM of 4 distinct si-hVDAC1 (2/A, A, B, C) or siRNA recognizing both murine and human VDAC1 (M/H) or with si-NT for 48 h and VDAC1 expression levels (F) and cell growth (G) were analyzed. (H-I) Mouse GL-261 and rat C6 cells were treated for 48 h with si-NT or si-VDAC1 (M/H) (75 nM) and then analyzed for VDAC1 levels (H) or cell growth (GL-261, gray bars and C6, white bars) using SRB (I).

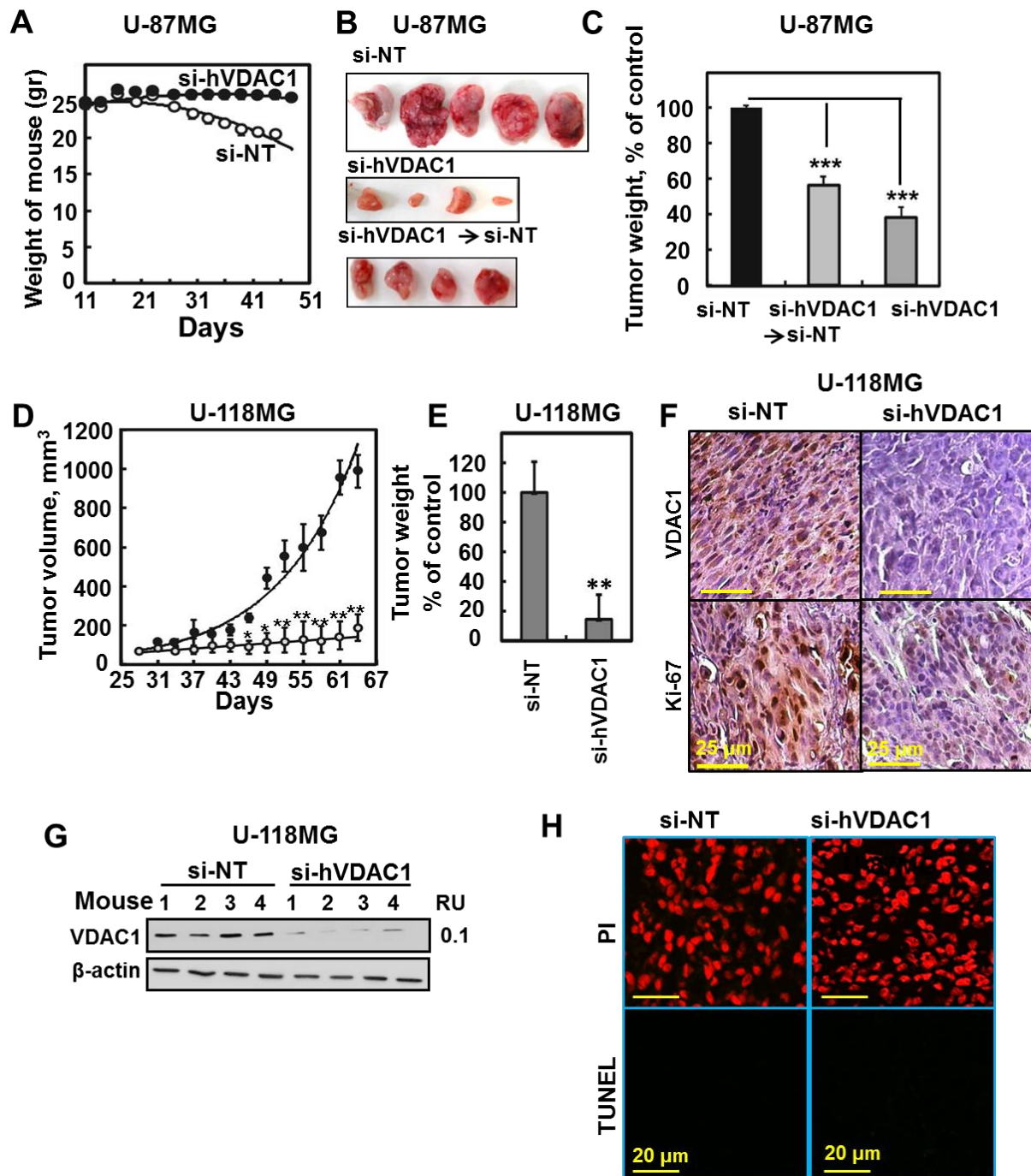


Figure S2. Inhibition of tumor development by si-hVDAC1 in U-87MG and U-118MG xenograph mouse models

(A) Mouse body weight of si-NT and si-hVDAC1 U-87MG xenograft-treated mice. (B, C) Dissected tumors (B) and the weight (C) of U-87MG cell xenografts treated with si-NT (black bar), si-hVDAC1 (dark gray bar) or si-hVDAC1 transferred into si-NT (light gray bar). The results show the mean \pm SEM (n = 8-16), (***)- $p < 0.001$). (D, E) U-118MG cells were s.c. inoculated into male athymic nude mice. On day 25, the mice were divided into 2 groups (average tumor volume, 60 mm³) and injected intratumorally every three days with si-NT (●, 5 mice) or si-hVDAC1(2/A) (○, 5 mice) to a final concentration of 50-60 nM. Differences in tumor volume (D) and weight (E) between si-NT- and si-hVDAC1(2/A)-TTs were highly significant (**- $p < 0.01$). (F) IHC representative sections from si-NT- and si-hVDAC1-TTs immunostained for VDAC1 and for Ki-67. (G) VDAC1 levels in si-NT- and si-hVDAC1-TTs as analyzed by immunoblotting. RU=average relative VDAC1 level. (H) Sections of paraffin-embedded U-87MG s.c. xenograft from si-NT- or si-hVDAC1-TTs stained with PI or TUNEL showing no cell death.

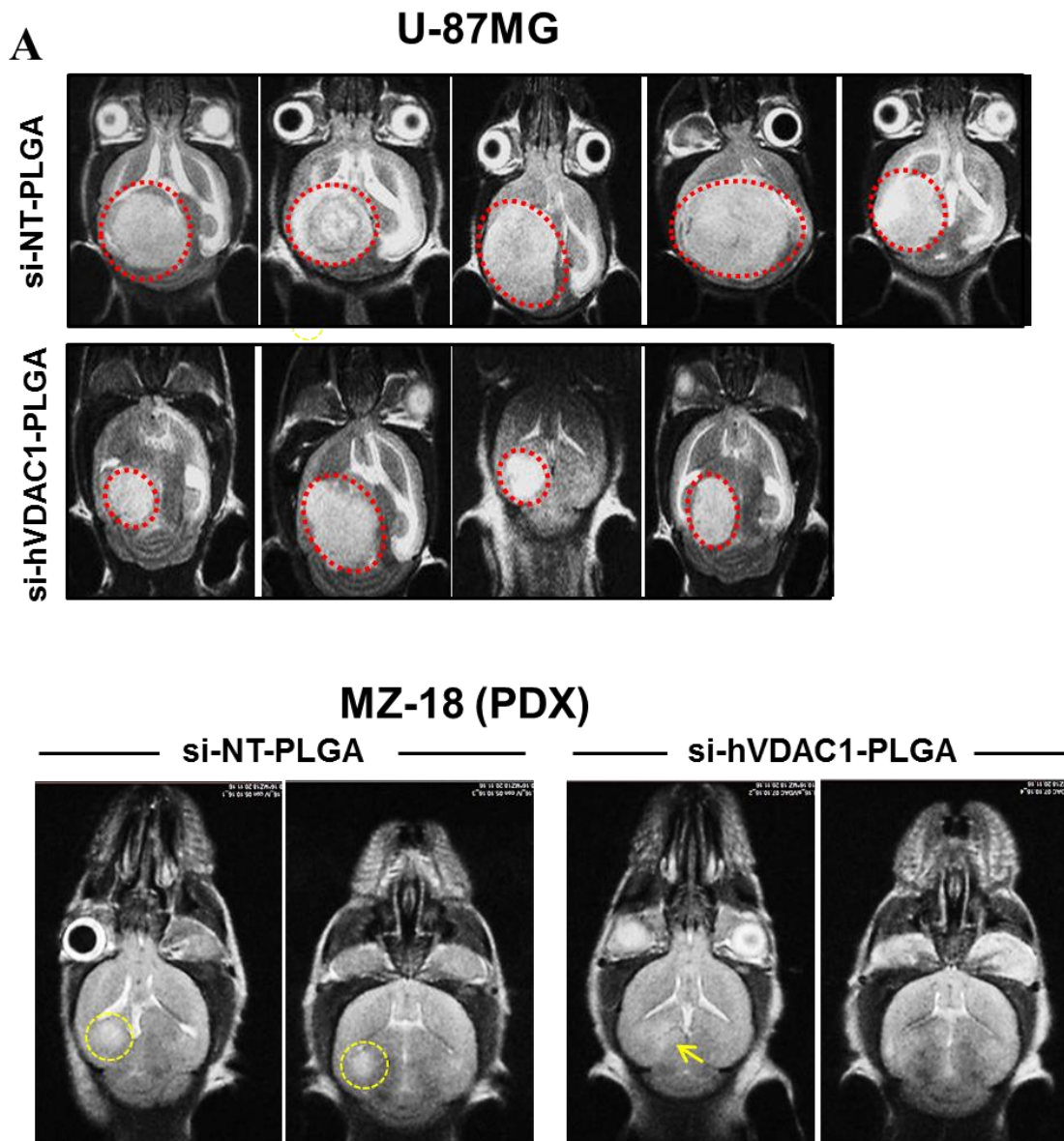


Figure S3. si-hVDAC1 inhibition of orthotopic GBM derived from U-87GBM or MZ-18 PDX cells
 Orthotopic GBM. (A) MRI imaging of brains engrafted with U-87MG cells (8×10^4) 30 days after engraftment. Two days post-enugraftment, the mice were divided into 2 groups (6 mice each) and injected i.v. every 3 days with 100 μ l of si-NT- or si-hVDAC-encapsulated PLGA-PEI nanoparticles (400 nM siRNA). (B) Similar experiment as in (A), using MZ-18 (PDX) cells (10×10^4). Two days post-enugraftment, the mice were divided into 2 groups (6 mice each) and injected i.v. with 100 μ l of si-NT- or si-hVDAC-encapsulated PLGA-PEI nanoparticles (400 nM siRNA). MRI imaging was carried out 45 days post-enugraftment and 10 days after treatment was terminated. Tumors are circled and arrow points to possible residual tumor.

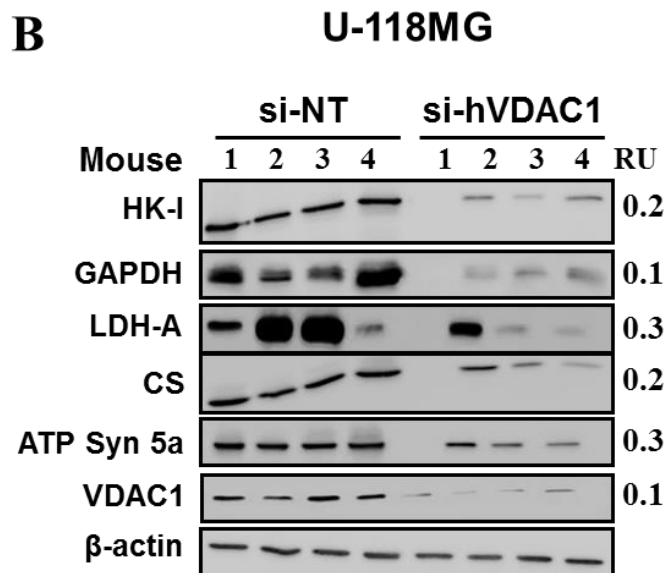
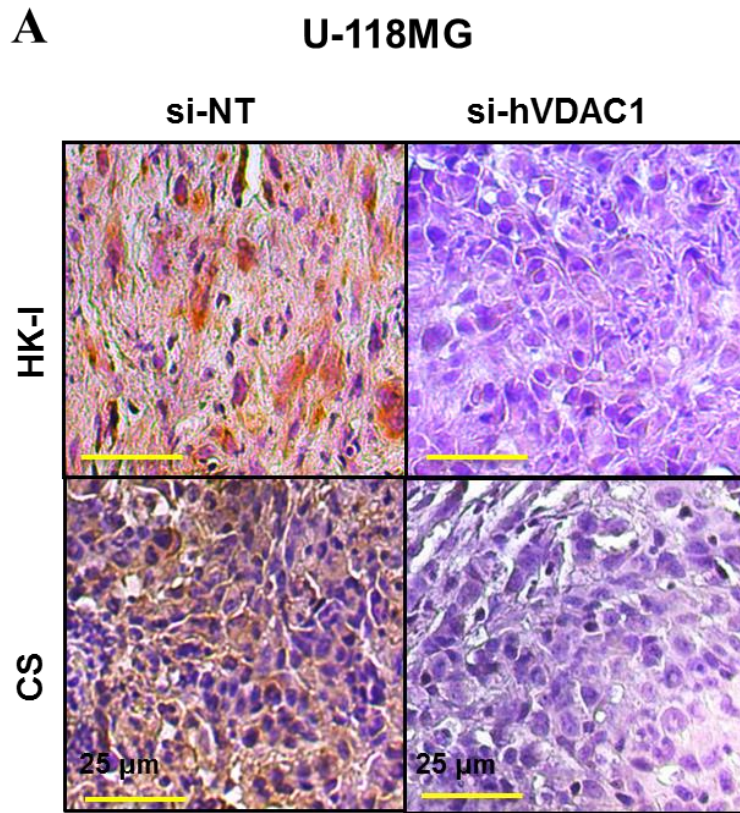


Figure S4. si-hVDAC1-TTs showed a reversal of reprogramed metabolism

U-118MG cell xenografts (s,c) treated with si-NT or si-hVDAC1 to a final concentration of 50 nM

(A) IHC staining of si-NT- or si-hVDAC1-TTs sections from s.c. U118MG-derived tumors using specific antibodies against HK-I and CS. (B) Immunoblot staining for HK-I, GAPDH, LDH-A, CS, ATP synthase 5a and VDAC1. β -actin immunostaining serving as a loading control is presented. RU = relative unit.

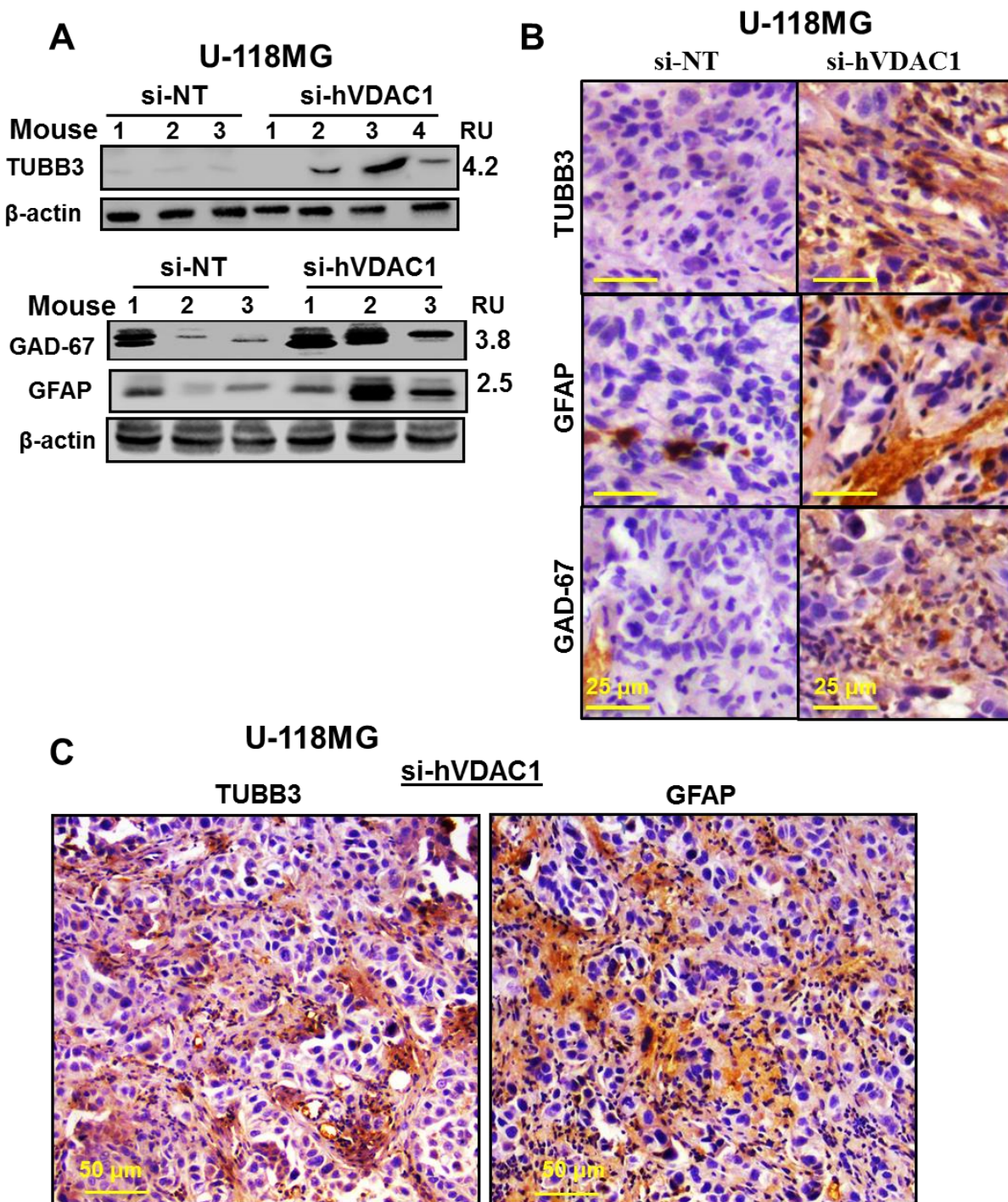


Figure S5. si-hVDAC1-TTs showed increased expression of differentiation markers

(A) Proteins extracted from s.c si-NT- or si-hVDAC1-TTs derived from U-118MG cells were immunoblotted for TUBB3, GFAP and GAD-67. β-actin immunostaining serving as a loading control is presented. RU=relative unit. (B) IHC staining of si-NT- or si-hVDAC1-TT sections from a U-118MG-derived tumor using specific antibodies against TUBB3, GFAP and GAD-67. (C) IHC staining of si-hVDAC1-TT for TUBB3 and GFAP.

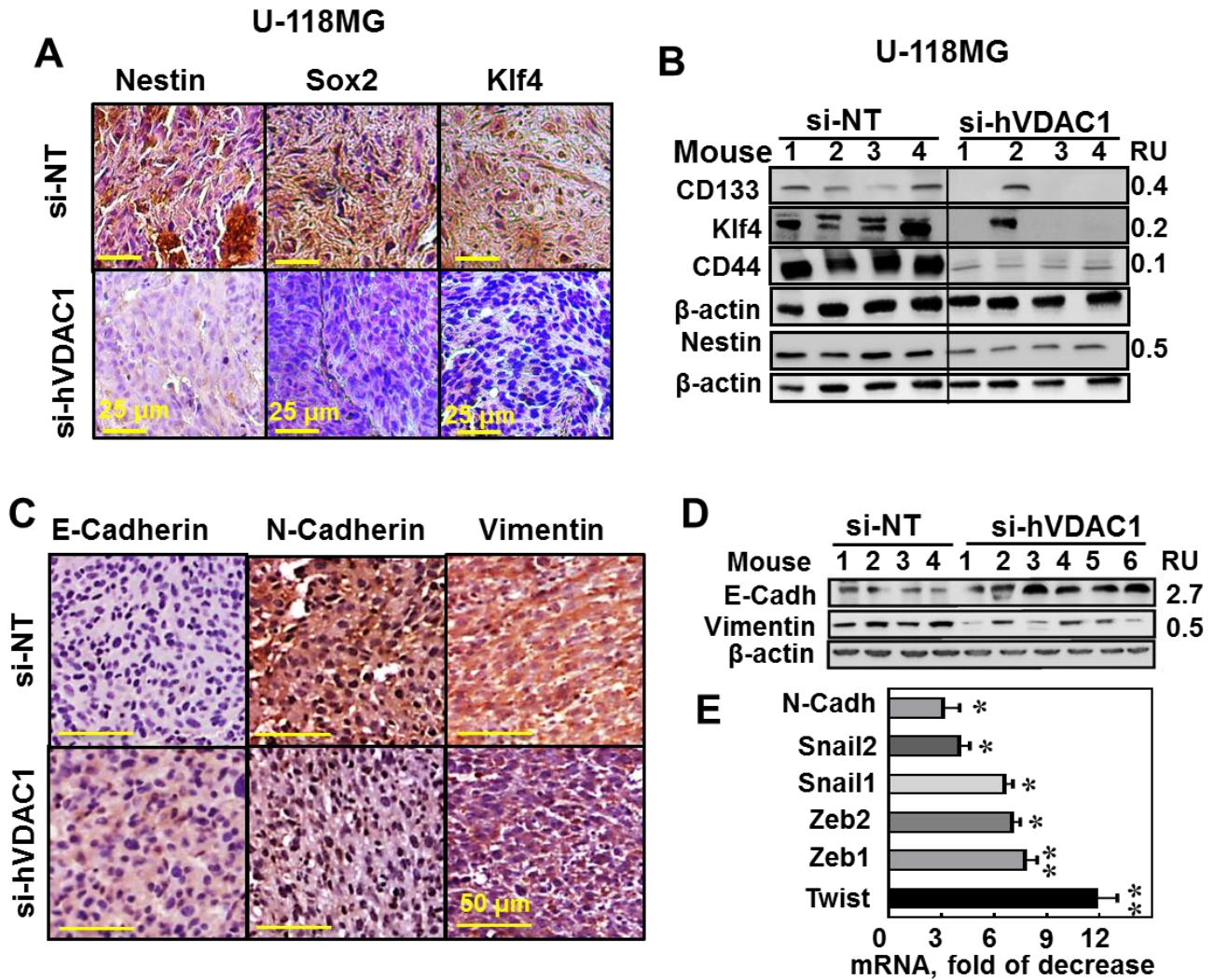


Figure S6. si-hVDAC1 treatment altered expression of stem cell and EMT markers

(A) IHC of si-NT- or si-hVDAC1-TT sections from U-118 tumors stained for the stem cell markers Nestin, Sox2 and Klf4. (B) Immunoblot analysis of CD133, Klf4, CD44 and Nestin levels in si-NT- and si-hVDAC1-TTs sections from U118MG-derived tumors. RU = average relative protein expression levels. IHC staining (C) and immunoblotting (D) of si-NT- and si-hVDAC1-TTs (s.c) sections from U-87MG tumors stained for E-cadherin, N-cadherin and vimentin. (E) qRT-PCR analysis of N-cadherin (N-Cadh), Snail1, SLUG, Zeb1, Zeb2 and Twist mRNA levels in si-NT- and si-hVDAC1-TTs. Results are the mean \pm SEM (n=3-5, p:* \leq 0.05; ** \leq 0.01). RU = average relative levels.

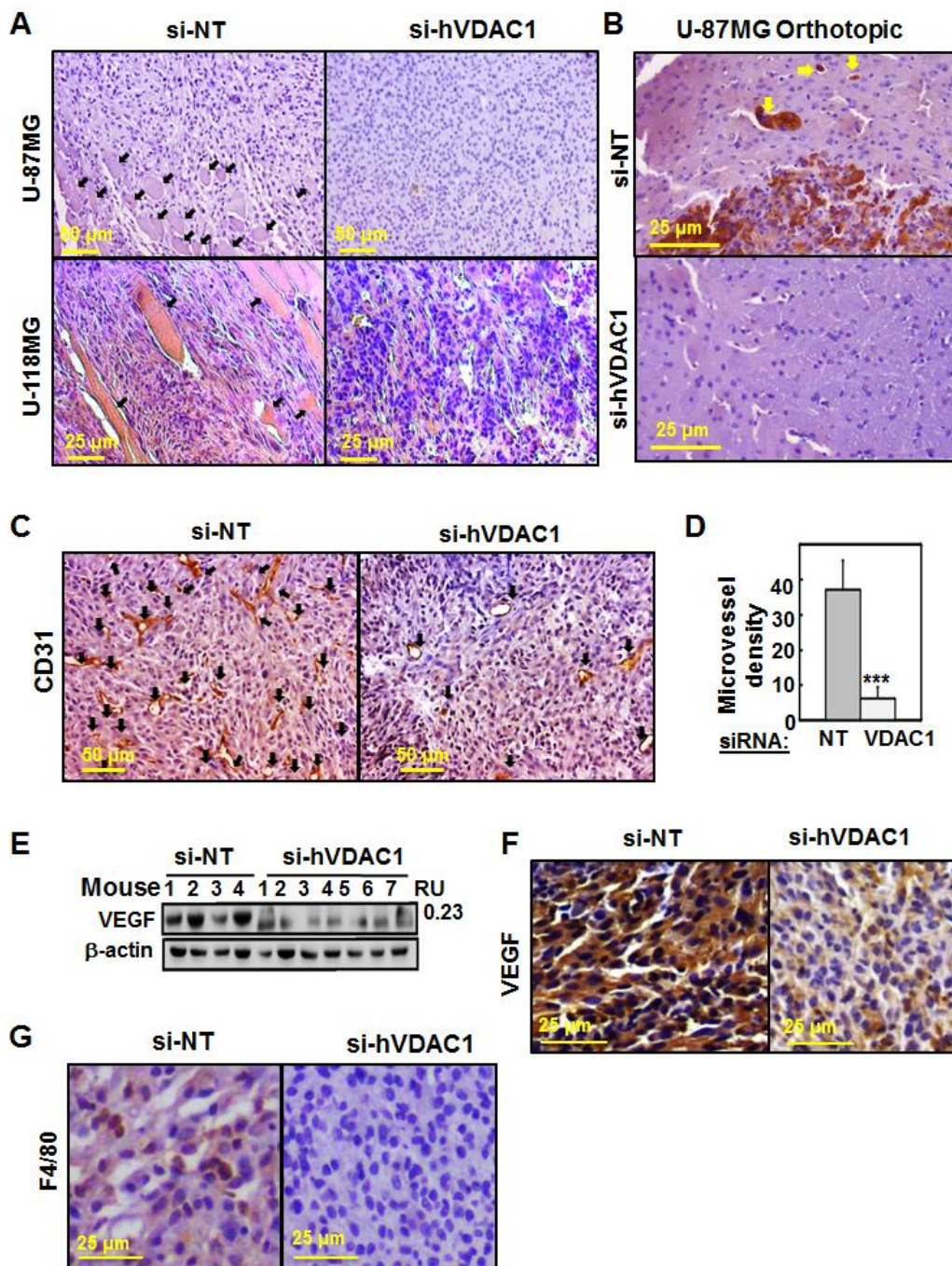


Figure S7. si-hVDAC1 tumor treatment inhibited invasion and angiogenesis

A) H&E staining of si-NT- and si-hVDAC1-treated U-87MG and U-118MG tumors, showing representative sections. Arrows point to muscle, indicative of tumor invasion. **(B)** Representative IHC staining for Nestin in sections from brains engrafted with si-NT- or si-hVDAC1-treated U-87MG cells, 22 days after cells engraftation. Arrows point to tumor invasion in the brain. **(C)** Representative IHC staining of blood vessels in sections from si-NT- and si-hVDAC1-TTs derived from U-87MG tumors, as revealed using anti-CD31 antibodies. Black arrows point to blood vesicles. **(D)** Quantitative analysis of microvessel density (MVD) per unit area expressed as means ± SEM, *** $p < 0.001$; si-NT versus si-hVDAC1 ($n = 5$ animals from each group). **(E-G)** Immunoblotting **(E)** and IHC staining of tumor sections derived from U-87MG tumors treated with si-NT- or si-hVDAC1 using anti-VEGF **(F)** or anti-F4/80 **(G)** antibodies.

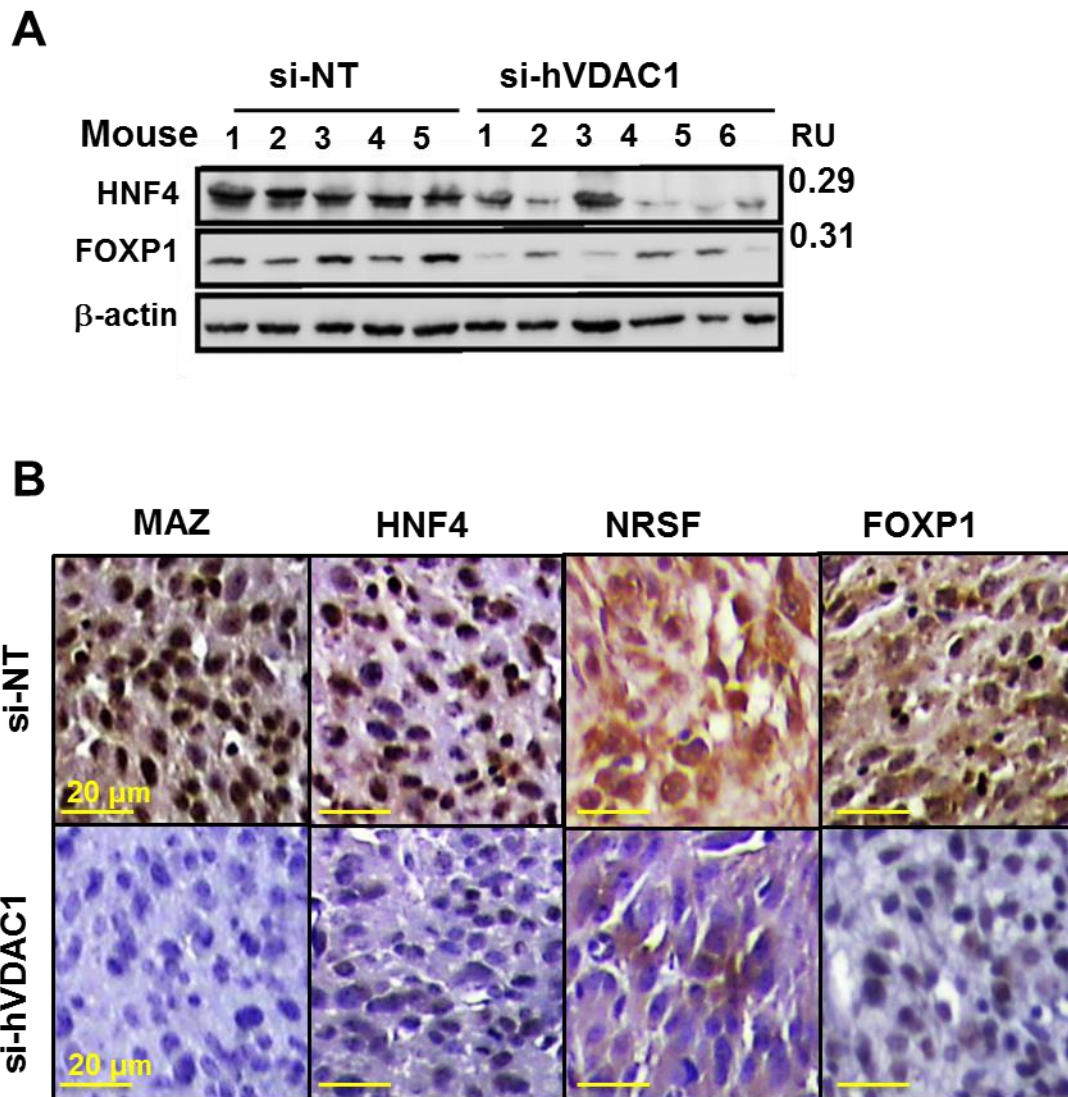


Figure S8. Altered expression levels of TFs FOXP1, NRSE, HNF4 and MAZ in si-hVDAC1- TTs
(A) Immunoblot of HNF4 and FOXP1 in si-NT- and si-hVDAC1-TTs. RU = Average relative level. **(B)** IHC staining of si-NT- or si-hVDAC1-TTs using antibodies specific to the TFs identified in A: FOXP1, NRSF, HNF4 and MAZ.

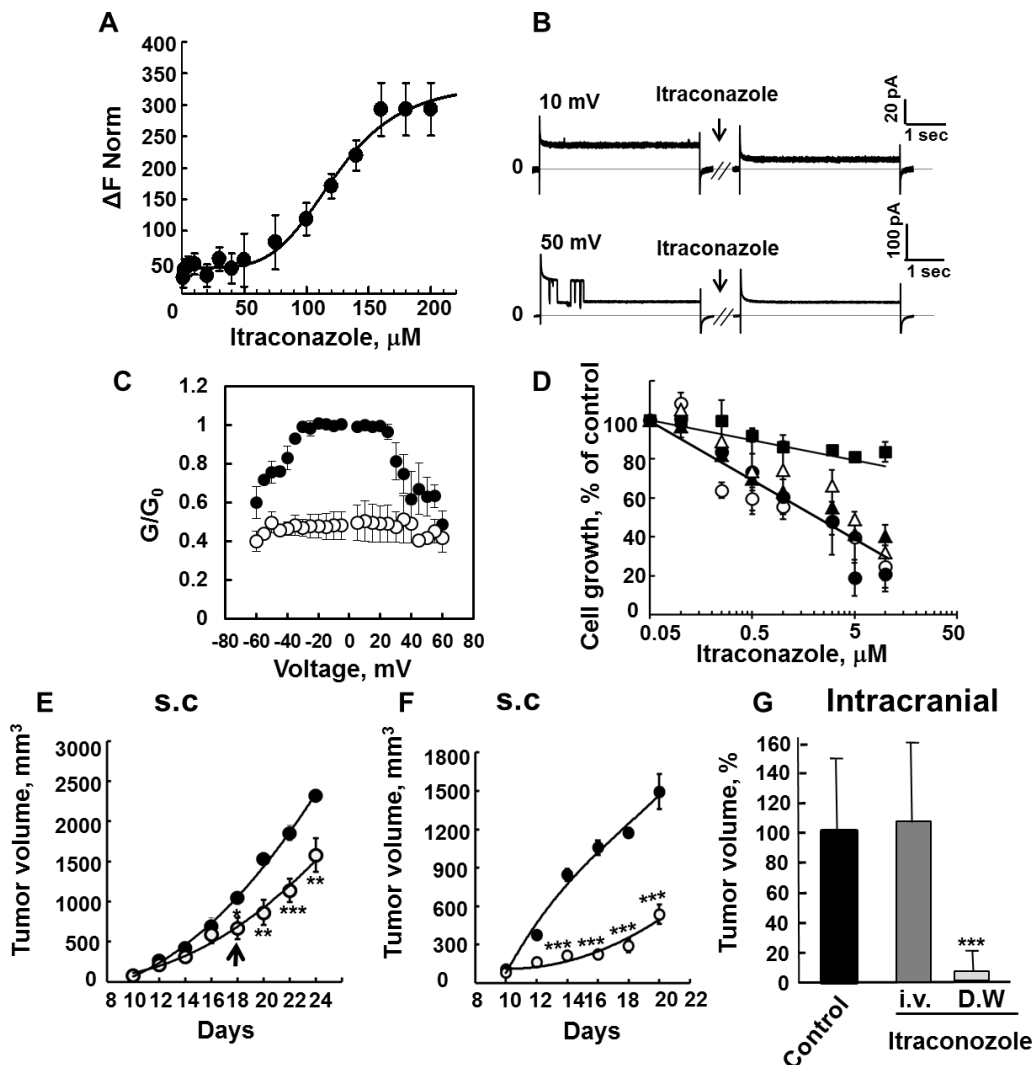


Figure S9. Itraconazole directly interacts with purified VDAC1 to reduce channel conductance and inhibit cell growth.

A. Purified VDAC1 (200 nM), labeled using the NanoTemper fluorescent protein-labeling Kit BLUE, was incubated with increasing concentrations of itraconazole. After 20 min of incubation, 3-5 μl of the samples were loaded into MST-grade glass capillaries and the thermophoresis process was measured using the Monolith-NT115 apparatus. The results are presented as the percent of the bound fraction, calculated as: $\text{Fraction bound} = 100 \times \frac{F - F_{\text{min}}}{F_{\text{max}} - F_{\text{min}}}$. **B.** Purified VDAC1 was reconstituted into a PLB and currents through VDAC1, in response to a voltage step from 0 to 10 mV, were recorded before and 30 min after the addition of 40 μM of itraconazole. **C.** Multi-channel recordings of VDAC1 conductance as a function of voltage, and the average steady-state conductance of VDAC1 before (o) and 30 min after the addition of itraconazole (\bullet). Relative conductance (G/G_0 , conductance/maximal conductance) was determined at a given voltage. The data were normalized according to the conductance obtained at -10 mV (maximal conductance). **D.** U-87MG (\bullet), U-118MG (o), LN-18 (\blacktriangle) and mouse PBCs (\blacksquare) grown in DMEM in 96-well plates (2000 cells/per well), and HUVEC (Δ) grown in complete EBM-2 were incubated for 24h with the indicated concentrations of itraconazole and then analyzed for cell growth using the SRB method ($n=3$). **E.** U-87MG cells were s.c. inoculated into male athymic nude mice. On day 10, the mice were divided into 2 groups (each 5 mice, average tumor volume, 80 mm^3) and injected intratumorally every two days with 5% glucose solution containing 5% DMSO (\bullet) or itraconazole (o) to a final concentration of 30 μM (**E**) or 100 μM (**F**). The arrow indicates a switch in itraconazole treatment from 30 to 100 μM . **G.** MZ-18 (PDX) cells were inoculated intracranially into the brain of female athymic nude mice. On day 5, the mice were randomly divided into 3 groups (5 mice each). The first and second groups were injected i.v. every two days with 5% glucose solution containing 5% DMSO or itraconazole (50 mg/kg). The third group received itraconazole in the drinking water (DW) (50 mg/kg). Tumor volume was calculated from MRI images taken 34 days post-cell engraftment, as described in the Materials and Methods section. Differences in tumor volume were significant (**- $p < 0.01$; *** ≤ 0.001).